JACS
JOURNAL OF THE AMERICAN CHEMICAL SOCIETY
Article
pubs.acs.org/JACS

Hydrogen Evolution from Pt/Ru-Coated p-Type WSe_2 Photocathodes

James R. McKone, Adam P. Pieterick, Harry B. Gray,* and Nathan S. Lewis*

Division of Chemistry and Chemical Engineering and the Joint Center for Artificial Photosynthesis, California Institute of Technology, 1200 East California Blvd, Pasadena, California 91125, United States

Supporting Information

ABSTRACT: Crystalline p-type WSe_2 has been grown by a chemical vapor transport method. After deposition of noble metal catalysts, p-WSe_2 photocathodes exhibited thermodynamically based photoelectrode energy-conversion efficiencies of >7% for the hydrogen evolution reaction under mildly acidic conditions, and were stable under cathodic conditions for at least 2 h in acidic as well as in alkaline electrolytes. The open circuit potentials of the photoelectrodes in contact with the H^+/H_2 redox couple were very close to the bulk recombination/diffusion limit predicted from the Shockley diode equation. Only crystals with a prevalence of surface step edges exhibited a shift in flat-band potential as the pH was varied. Spectral response data indicated effective minority-carrier diffusion lengths of ~1 μm, which limited the attainable photocurrent densities in the samples to ~15 mA cm^{-2} under 100 mW cm^{-2} of Air Mass 1.5G illumination.

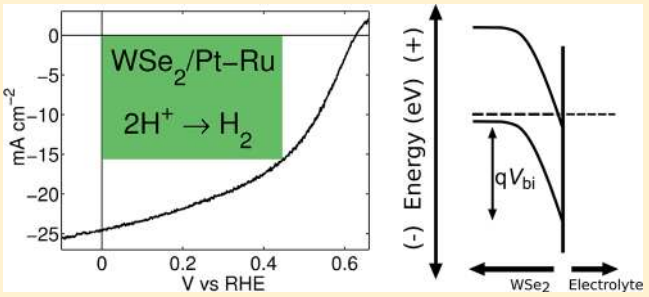

INTRODUCTION

The production of solar fuels would provide a globally scalable solution to the storage problem associated with the regional intermittency of sunlight.[1−4] Possible solar fuels systems include water splitting to produce H_2 and O_2, as well as the cathodic reduction of CO_2 to carbonaceous species such as CO, CH_3OH, and CH_4, accompanied by the anodic oxidation of water to O_2. Efficient H_2 evolution has been demonstrated in 1.0 M HCl(aq) for single crystals of p-InP coated with a series of noble metal electrocatalysts,[5,6] as well as by Pt-coated n^+-p radial junctions formed from Si microwire arrays in 0.5 M H_2SO_4(aq).[7] By analogy to conventional electrolysis, photoelectrolysis is especially attractive in either acidic or alkaline media, where the conductivity of aqueous electrolyte is largest, and where suitable membranes are available to neutralize the pH gradient while preventing deleterious product crossover that would reduce the system efficiency and possibly create an explosive mixture of H_2 and O_2 in the system.[8,9] Neither Si nor InP is chemically stable in alkaline environments, so the identification of a photocathode material that can offer high energy-conversion efficiency while being stable in alkaline conditions would expand the available options for assembly of a functional solar-fuels generation system.

Semiconducting tungsten and molybdenum chalcogenides have been previously studied for hydrogen-evolution applications. Tungsten disulfide, with a band gap of 1.4 eV, has been explored as a photocathode for hydrogen evolution, exhibiting open-circuit potential shifts as high as ~850 mV relative to the hydrogen electrode potential, and with noble metal cocatalysts demonstrating energy-conversion efficiencies exceeding 10% under low light intensity in strongly acidic solution.[10,11] SiO_2-supported polycrystalline WS_2 has been shown to effect the stable production of H_2 for several days under either acidic or alkaline conditions, in the presence of V^{2+} or CdS as a sensitizer.[12] Molybdenum disulfide has also been reported to be a highly active electrocatalyst for hydrogen evolution in acidic solution, with reported exchange current densities on the order of 10^{-5} A cm^{-2}, and activities on a per site basis that approach those of the noble metals.[13−18] Tungsten and molybdenum chalcogenides oxidize when polarized near the oxygen-evolution potential,[19,20] but single crystalline photoelectrodes have been shown to be extremely stable when operated under moderately oxidizing conditions.[21] Hence, it is possible that this family of photoelectrode materials could afford stability under alkaline as well as acidic conditions, and could also exhibit excellent energy-conversion efficiencies either on bare electrode surfaces or when coupled to active electrocatalysts for the production of H_2 from water.

Tungsten diselenide was studied extensively through the 1980s as a compound semiconductor photoanode, owing to its high light absorption coefficient, 1.2 eV band gap, and anisotropic properties that are a consequence of its layered structure.[22,23] Crystalline n-type WSe_2 has exhibited stability as well as >17% photoelectrochemical energy-conversion efficiency in contact with aqueous polyhalide-based redox systems.[19,21,24−33] Given the impressive performance of n-type WSe_2 photoanodes, p-type WSe_2 is an attractive target material for effecting efficient photoelectrochemical hydrogen evolution. Thus, we report herein the synthesis and photoelectrochemistry of crystalline p-type WSe_2 photocathodes. We specifically describe the optical and photoelectrochemical

Received: August 29, 2012
Published: November 30, 2012

 © 2012 American Chemical Society dx.doi.org/10.1021/ja308581g | J. Am. Chem. Soc. 2013, 135, 223−231

properties of p-WSe_2 in contact with one-electron, reversible redox couples, as well as the photoelectrochemical behavior in contact with the aqueous hydrogen evolution redox couple at various pH values, with and without surface-attached electrocatalysts.

EXPERIMENTAL SECTION

Crystal Synthesis. Crystals of WSe_2 were grown by a chemical vapor transport technique.[21,34−38] A stoichiometric mixture of elemental W and Se was first loaded into a ∼25 mm inner diameter quartz ampule. The ampule was vacuum-sealed and heated overnight at ∼900 °C to form polycrystalline WSe_2. A 1.25 g quantity of polycrystalline WSe_2 was then loaded into a 14 mm inner diameter quartz ampule, along with 0.38 g of WO_2Cl_2, 0.18 g of Se metal, and ∼5 mg of Nb powder. The ampule was sealed under vacuum and heated for 24 h to 1000 °C in the growth zone and 950 °C in the charge zone. The temperature gradient was then reversed, producing a temperature of 950 °C in the growth zone and 1000 °C in the charge zone, with a gradient of ∼2 °C cm^{-1}. After 3 days, several thin, smooth, black hexagonal plates of crystalline WSe_2, as large as 5−7 mm on a side, were obtained.

Several (>10) growths of crystalline WSe_2 were attempted using the above methodology. Each growth yielded crystalline material, but only a few growths produced a large quantity of crystals that were of the appropriate size and electronic quality for use in photoelectrochemical experiments. All samples described herein were taken from a single growth run, to ensure consistent materials properties across all of the reported experiments.

Preparation of Photoelectrodes. To prepare electrodes, WSe_2 crystals were first cleaved into pieces ∼2−3 mm on a side, by placing the parent crystal on a glass slide and carefully cutting the sample with a sharp razor blade. The pieces were mounted onto Cu wires by either scratching Ga/In eutectic into one side of the WSe_2 using a tungsten carbide scribe and then using Ag paint to attach the crystal to the Cu wire, or by using In metal to solder the crystals directly to a Cu wire. Both methods produced ohmic contacts that were suitable for DC and AC electrochemical analyses. The mounted electrodes were then cleaved of one or several surface layers by careful peeling with adhesive tape. These cleaved samples contained a variety of apparent step edge densities, as observed by optical or electron microscopy. The electrode surface was then defined by sealing the back and edges with two-part epoxy (Hysol 9460).

Electrochemistry. DC and AC electrochemical analyses were performed using a Gamry Reference 600 potentiostat. For photoelectrochemistry, illumination was provided by an ELH-type tungsten-halogen bulb whose intensity was set on the plane of the sample to produce the same current density on a calibrated Si photodiode as was obtained from 100 mW cm^{-2} of Air Mass 1.5 Global (AM1.5G) solar illumination. The Si photodiode (Thorlabs) had been calibrated relative to a NIST-traceable standard (Solarex). The spectral qualities of this light source have been previously characterized and provide an approximation of the AM1.5G solar spectrum.[39] The Supporting Information includes a comparison of the ELH-type tungsten-halogen bulb spectrum and the AM1.5G solar spectrum.

Current density vs potential (J−E) data were collected in contact with the reversible redox couple ruthenium hexammine ($Ru(NH_3)_6^{3+/2+}$) (chloride salt) using a single-compartment cell that consisted of a Pt counter electrode along with a glassy carbon pseudoreference that was poised at the solution potential. Potassium phosphate was used as the supporting electrolyte and pH buffer at pH = 2.25. The solution was agitated by vigorous magnetic stirring and was continually purged by a flow of N_2(g). The solution potential was established by bulk electrolysis, using a porous carbon working electrode and a Pt counter electrode separated by a fritted compartment, until the solution reached −0.1 V vs the saturated calomel electrode (SCE), as measured by the glassy carbon pseudoreference electrode.

Stability data were collected for photoelectrodes in contact with a 50 mM $MV^{2+/+}$(aq) solution that had 0.5 M potassium phosphate to provide both a buffer and a supporting electrolyte. For measurements at pH = 2 or 10, a p-type WSe_2 electrode was submersed in the electrolyte and polarized at −0.600 V or −0.650 V vs SCE, respectively, while illuminating the sample with a tungsten-halogen lamp at ∼100 mW cm^{-2} of light intensity. Current vs time data were collected for 2 h in each solution. Before, between, and after testing in acidic and in alkaline media, the WSe_2 crystal surface was imaged using an optical microscope (Olympus BX51), to observe any changes in the surface morphology that resulted from corrosion of the photoelectrode.

The hydrogen evolution J−E data for WSe_2 electrodes that had been coated with noble metal cocatalysts were collected in either 0.5 M H_2SO_4(aq) or 0.5 M K_2SO_4(aq) with 0.2 M potassium hydrogen phthalate (KHP) buffer at pH 4.2. Measurements were performed using a two-compartment electrochemical cell, with a Pt mesh counter electrode that was separated from the main compartment by a fine porosity frit. The reference electrode was either a $Hg/HgSO_4$ (acid electrolyte) electrode or a SCE (KHP electrolyte). J−E data were collected while the solution was actively purged with H_2(g) (AirLiquide, Alphagaz 2) at 1 atm of pressure, and with vigorous stirring. The electrochemical potentials were referenced to the RHE potential in the electrolyte of interest, which was measured using a clean Pt wire electrode.

Spectral response data were obtained using a 50 mM aqueous solution of only the optically clear, oxidized form of the $MV^{2+/+}$ along with 0.5 M K_2SO_4 and 0.2 M KHP at pH = 4.2. Between experiments, the solution was reoxidized by stirring in air, to minimize light absorption by the intensely colored MV^+ radical cation species. The electrode potential was held at −0.400 V vs SCE. The light source was a Xenon lamp, chopped at 13 Hz, and the illumination wavelength was scanned in 10 nm steps from 1050 to 350 nm.

Differential capacitance vs potential (C_{diff}−E) data were collected in contact with 200 mM $Fe(CN)_6^{3-/4-}$ (potassium salts) solutions of varying pH that contained equal concentrations of the oxidized and reduced forms of the redox species. The supporting electrolytes and pH buffers for three different solutions were 0.5 M potassium phosphate adjusted to pH values of 2.5, 6.6, or 10.2, respectively. The C_{diff} values were calculated from the imaginary component of the impedance at the potential of interest, and the data were processed according to an established procedure to produce Mott−Schottky plots (see Supporting Information).

Catalyst Deposition. Ru and Pt were deposited by a photoelectrochemical method that was similar to an approach used previously for InP photoelectrodes.[5] To deposit Ru, electrodes were placed in a solution of 0.1 mM $RuCl_3$ and 0.1 M HCl, illuminated under ∼1 Sun intensity, and biased for several min potentiostatically at −0.100 V vs SCE. During this time, the current flow increased due to the onset of hydrogen evolution that was catalyzed by the depositing Ru film. Deposition of Pt was performed using the same procedure, but with 1 mM H_2PtCl_6 in 0.1 M HCl(aq) and with the illumination manually chopped at ∼1 Hz.

To deposit the mixed Ru−Pt catalyst, Ru was deposited as above, and then the photoelectrodes were briefly rinsed and placed in a 50 mM solution of H_2PtCl_6(aq) for 5−20 s. The electrodes were then removed, thoroughly rinsed and dried, and tested for hydrogen evolution activity under illumination.

Efficiency Calculations. Photoelectrode efficiencies for conversion of solar energy to hydrogen were calculated on a thermodynamic basis using the solution potential (i.e., RHE) as a reference. The RHE potential in the electrolyte of interest was determined explicitly by measurement of the open-circuit potential of a freshly cleaned Pt wire relative to a mercury sulfate or to a saturated calomel reference electrode, while purging the system with 1 atm of research grade H_2(g). The photoelectrode energy-conversion efficiency η was calculated as in eq 1:

$$\eta = \frac{J_{Pmax} \cdot V_{Pmax}}{P_{in}} \quad (1)$$

dx.doi.org/10.1021/ja308581g | J. Am. Chem. Soc. 2013, 135, 223−231

where J_{Pmax} and V_{Pmax} are the current density and photovoltage (relative to RHE) at the maximum power point and P_{in} is the incoming light flux (100 mW cm^{-2} for 1-Sun intensity). These calculated photoelectrode efficiencies do not correct for losses due to concentration overpotentials, kinetic overpotentials, or any uncompensated resistance losses in the cell. Thus, they are underestimates relative to the "power saved" or photovoltaic efficiencies that would be calculated with respect to the voltage needed for a purely electrocatalytic cathode to produce the same current density for H_2 evolution in the same electrolyte.[5,6] The use of the RHE potential as the reference potential is directly analogous to the use of the Nernst or solution potential in the photoelectrode efficiency calculation for a semiconductor electrode in contact with a nonaqueous electrolyte that contains outer-sphere, kinetically facile, 1-electron redox couples. Further discussion of the efficiency calculations is included in the Supporting Information.

RESULTS

Hydrogen Evolution. Figure 1 displays $J-E$ data under illumination for representative p-type WSe_2 electrodes with or without Pt, Ru, and Ru/Pt at pH = 4.2. Without deposition of a catalyst, the WSe_2 crystals exhibited negligible current for electrode potentials E > RHE, indicating that such photocathodes produced negligible net conversion of light energy to H_2(g). Upon deposition of a noble metal catalyst, however, the p-WSe_2 electrodes produced significant cathodic current density for E > RHE, displaying photocurrent densities, J_{ph}, that reached >25 mA cm^{-2}, and values of J at E = 0 V vs RHE (the short-circuit current density, J_{sc}) that reached >24 mA cm^{-2} of cathodic current density in the best-performing electrode measured to date.

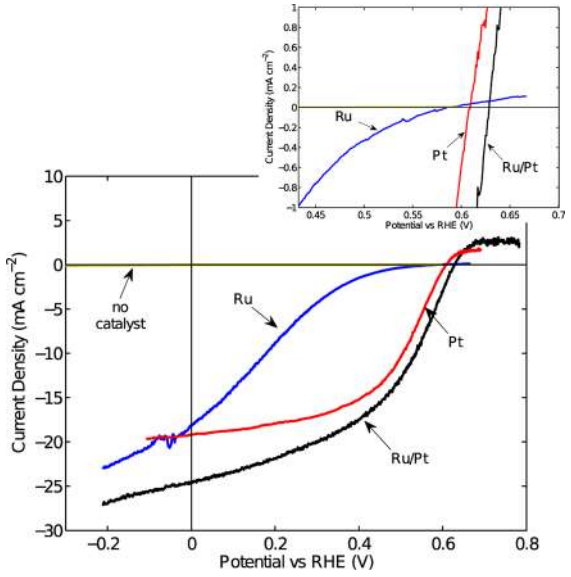

Figure 1. $J-E$ behavior of p-WSe_2 photoelectrodes generating H_2(g) from aqueous pH 4.2 electrolyte without catalyst coating and with Ru, Pt, or Ru/Pt coatings, respectively. All electrodes were illuminated using an ELH tungsten halogen lamp calibrated to an equivalent of 100 mW cm^{-2} intensity using a Si photodiode. The inset is a detail of the region around the open-circuit potential of the photoelectrodes.

The inset of Figure 1 shows a detailed view of the $J-E$ behavior in the potential region near open-circuit. The open-circuit voltage (V_{oc}) values for the various p-WSe_2/catalyst combinations varied in the order: [no catalyst] < Ru < Pt < Ru/Pt. Ru-coated samples exhibited a significantly slower increase of current as the potential became more negative relative to the open-circuit potential, E_{oc}, resulting in low energy-conversion efficiencies for such systems. Table 1 lists photoelectrode hydrogen-evolution figures of merit for several high-performing WSe_2 electrodes, identified by electrode number. Full results are tabulated in the Supporting Information. The champion electrode, labeled 459 in Table 1, was first coated with a Ru cocatalyst and tested, and then coated with Ru/Pt and tested again. After the Ru/Pt deposition, this electrode produced >7% thermodynamically based photoelectrode energy-conversion efficiencies under the specific test conditions.

Table 1

electrode #	catalyst	electrolyte[a]	V_{oc} (mV)	J_{sc} (mA cm^{-2})	fill factor	efficiency (%)
412	Ru	KHP	660	−16.3	0.31	3.3
400	Pt	KHP	610	−19.2	0.53	6.2
415	Pt	KHP	570	−20.3	0.44	5.1
463	Ru/Pt	H_2SO_4	525	−20.5	0.53	5.6
464	Ru/Pt	H_2SO_4	610	−22.1	0.52	7.0
458	Ru/Pt	KHP	635	−21.7	0.45	6.1
459	Ru/Pt	KHP	630	−24.5	0.46	7.2

[a]KHP refers to 0.5 M K_2SO_4 buffered with 0.2 M potassium hydrogen phthalate at pH ~4.2; H_2SO_4 refers to 0.5 M sulfuric acid.

Figure 2 shows representative $J-E$ behavior under 100 mW cm^{-2} illumination of a single p-WSe_2 photoelectrode with a Ru/Pt cocatalyst under strongly acidic (0.5 M H_2SO_4) conditions as well as under mildly acidic (0.2 M KHP, pH 4.2) conditions. The shapes of the $J-E$ data were similar in both cases, with significant cathodic current flow in the power-producing region, i.e., for E > RHE. Under strongly acidic conditions, the photoelectrode exhibited more rapid onsets of both cathodic and anodic currents at potentials near E_{oc}. However, the electrode exhibited ~100 mV smaller V_{oc}, as well as a somewhat smaller limiting photocurrent density, in sulfuric acid than in the pH 4.2 electrolyte.

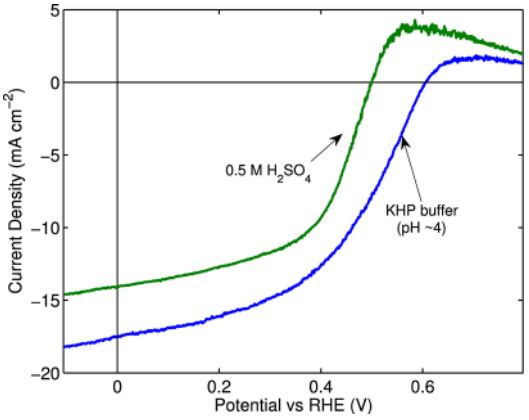

Figure 2. Current density vs potential behavior of a single illuminated p-WSe_2 photoelectrode coated with Ru/Pt catalyst at two different pH values. Illumination was provided by an ELH tungsten-halogen light source calibrated to an equivalent of 100 mW cm^{-2} intensity using a Si photodiode.

Reversible Electrochemistry. Figure 3 shows the $J-E$ behavior of a bare p-WSe_2 photoelectrode in contact with 50 mM $Ru(NH_3)_6^{3+/2+}$(aq). The reversible potential of the solution was −0.10 V vs SCE. The V_{oc} and J_{sc} values were close to those observed for H_2 evolution from Pt/Ru-coated p-

dx.doi.org/10.1021/ja308581g | J. Am. Chem. Soc. 2013, 135, 223−231

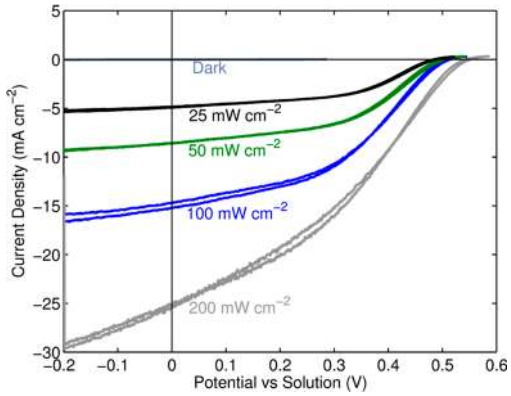

Figure 3. Current density vs potential behavior of an illuminated p-WSe_2 electrode without catalyst coating in 50 mM $Ru(NH_3)_6^{3+/2+}$ solution at pH 2.25 (0.5 M phosphate). Illumination from a tungsten halogen light source was calibrated to an equivalent of 100 mW cm^{-2} using a Si photodiode and modulated to the other noted intensities by adding or removing 0.3 optical density neutral density filters.

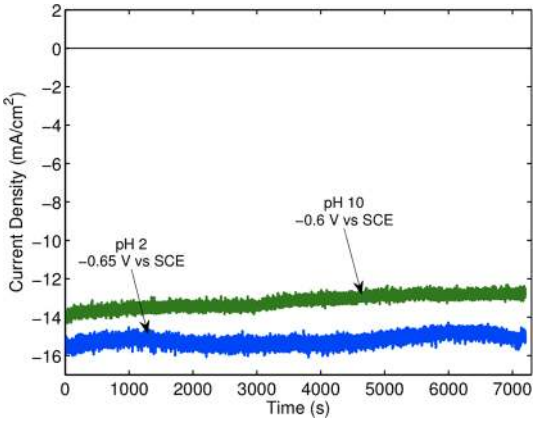

Figure 4. Current density vs time behavior of an illuminated p-WSe_2 photoelectrode submersed in a 50 mM solution of methyl viologen dichloride, buffered to pH 2 or 10 using 0.5 M potassium phosphate, and poised at the indicated potentials for 2 h.

WSe_2 photocathodes in 0.5 M H_2SO_4 (Figure 1); however, the fill factors were somewhat lower than in the fuel-forming case.

Stability Testing. To provide a cursory indication of electrode stability under cathodic bias in acidic or in alkaline media, a p-WSe_2 electrode was placed sequentially in contact with two different 50 mM $MV^{2+/+}$ solutions, at pH 2 and 10, respectively. In each case, the electrode was polarized under illumination at a potential sufficient to produce >10 mA cm^{-2} of cathodic current density (Figure 4). Figure 5 presents optical microscopy images of the WSe_2 crystal surface before, between, and after the stability tests.

Under acidic conditions, the electrode showed a slight decay in current density, from −15.5 to −15.0 mA cm^{-2}, over the course of the stability test. Under alkaline conditions, the current density decayed from −14.0 to −12.5 mA cm^{-2}. The optical micrographs showed the emergence of some visible cracks after the initial stability test in acid, and then no further notable change was observed after the test in alkaline media.

Mott–Schottky Analysis. Figures 6 and 7 display the C_{diff}–E data for two different WSe_2 photoelectrodes at various

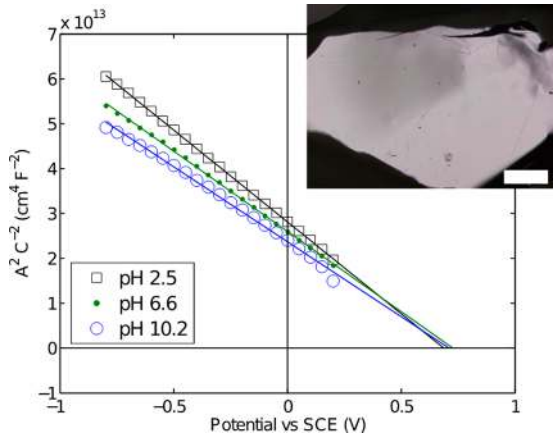

Figure 6. Mott–Schottky data collected in 200 mM $Fe(CN)_6^{3-/4-}$ solution at three different pH values (0.5 M potassium phosphate solutions) for a p-WSe_2 electrode exhibiting pristine surface morphology. The inset is an optical microscope image of the electrode (scale bar 0.5 mm).

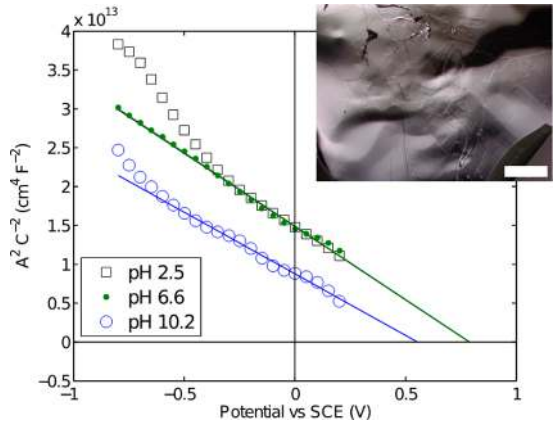

Figure 7. Mott–Schottky data collected as in Figure 6 for a p-WSe_2 electrode exhibiting a stepped surface morphology. The inset is an optical microscope image of the electrode (scale bar 0.5 mm).

Figure 5. Optical micrographs of the same portion of a p-WSe_2 crystal surface before stability testing (left), after testing under acidic conditions (center), and after testing under alkaline conditions (right). Scale bars are 0.2 mm.

dx.doi.org/10.1021/ja308581g | J. Am. Chem. Soc. 2013, 135, 223–231

pH values, in contact with $Fe(CN)_6^{3-/4-}(aq)$. The insets show optical micrographs of the crystal surfaces, illustrating the significant difference in step-edge density that was observed between the two samples. In reverse bias, both data sets showed a linear dependence of C_{diff}^{-2} vs potential over a range of several hundred millivolts. The slopes of the lines indicated p-type doping on the order of 10^{18} cm^{-3}, based on a relative dielectric constant of 4.5.[40]

The flat-band potential, E_{fb}, of the p-WSe_2 photoelectrode that was used to obtain the data in Figure 6 showed essentially no dependence on pH. For the electrode in Figure 7, negligible flat-band shift for pH values 2.5−6.6 was also observed, but the stepped electrode showed a shift in E_{fb} of ∼200 mV for pH values from 6.6 to 10.2. The dependence of the flat-band potential on pH was consistently larger for electrodes that exhibited a high prevalence of surface step edges that were evident by eye or under an optical microscope (see Supporting Information).

Spectral Response. Figure 8 depicts the external quantum yield (Φ_{ext}) of p-WSe_2/$MV^{2+/+}$ contacts vs excitation wavelength, along with vertical dashed lines that correspond to the indirect and direct band gap transitions of WSe_2 at 1.2 and 1.4 eV, respectively.[41] Integration of the observed spectral response data over the known photon flux of an ELH-type tungsten-halogen bulb at an intensity that produced the same photocurrent density on a Si photodiode as 100 mW cm^{-2} intensity of AM1.5G illumination yielded a predicted photocurrent density under ELH illumination of ∼19 mA cm^{-2}, which agrees with the range of short-circuit current densities that was observed for hydrogen evolution. Integration over the standard AM1.5G spectrum yielded a predicted photocurrent density of ∼15 mA cm^{-2} at an intensity of 100 mW cm^{-2}, consistent with the known difference in spectral distribution between the ELH lamp and the standard AM1.5 spectrum (see Supporting Information).[39]

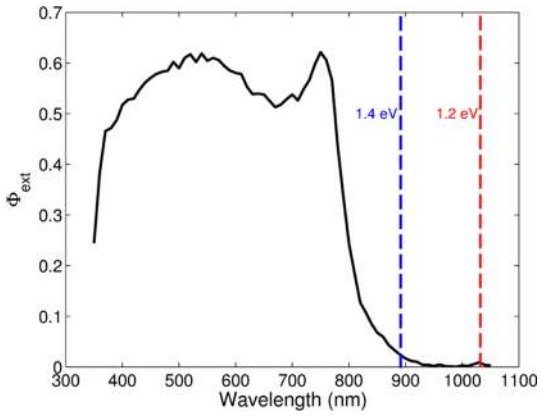

Figure 8. Spectral response data for a p-WSe_2 photoelectrode collected in clear methyl viologen solution. Vertical dashed lines at 1.2 and 1.4 eV correspond to the indirect and direct band edge transitions in WSe_2, respectively.

To estimate the effective minority-carrier diffusion length, L_D, the quantum yield data were fit to the Gärtner model of carrier diffusion (see Supporting Information), using absorption coefficient data reported previously, along with an estimated depletion width of 50 nm.[19] Figure 9 presents normalized Φ_{ext} values for L_D = 0.5, 1, or 2 μm calculated from the Gärtner model overlaid on the experimental results. The calculated values corresponding to L_D = 1 μm clearly produced the best fit to the experimental data.

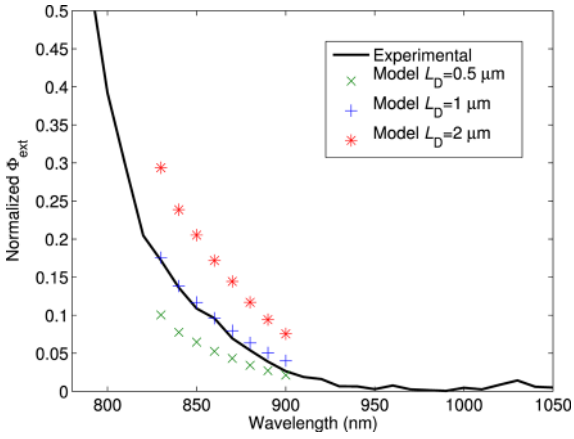

Figure 9. Spectral response data, normalized to the maximum Φ_{ext} value, in the onset region of >780 nm. The Gärtner-modeled points are for L_D values of 0.5, 1, or 2 μm.

DISCUSSION

Crystal Growth. Chemical vapor transport methods have been used previously to produce crystalline WSe_2.[34−37] In nearly all cases, a halide transport agent was provided either by addition of pure halogen or by a compound that thermally decomposed to yield a halogen. A thermodynamic analysis of the transport of tungsten and sulfur species by chlorine, to form crystalline WS_2, has indicated that the primary transport species is WO_2Cl_2 rather than the more volatile metal halide species.[34] This thermodynamic analysis implies that small amounts of oxygen are necessary to allow efficient transport and crystallization of group VI chalcogenide crystals. In our work, the putative transport species was explicitly included in the growth ampule, to ensure an adequate supply of oxygen and halogen. This method proved to be convenient, because tungsten oxychloride can be handled on the benchtop even though it is somewhat moisture sensitive.

Nb and V have been used to produce p-type doping in WSe_2, but often at the expense of crystal quality.[36,37] The use of WO_2Cl_2 as a chlorine-containing transport species, along with Nb in the growth ampule, consistently yielded p-type doping of WSe_2, while maintaining reasonable crystal size and quality. Interestingly, the quantity of Nb in the growth ampule (1 mol %) was much larger than the amount required to produce significant p-type doping in a semiconductor crystal. Baglio et al. concluded from their thermodynamic analysis that tungsten chalcogenide growth can accommodate an excess of niobium dopant in the starting material, due to the low concentration of volatile niobium species during the transport and crystal growth reaction.[34]

Solar Energy Conversion to H_2(g). Tungsten diselenide crystals with n-type doping have demonstrated high solar energy-conversion efficiencies in regenerative photoelectrochemical cells, especially after treatment of the photoelectrodes by surface preparation techniques that were intended to passivate surface recombination sites.[30,31] However, relatively few studies have assessed the efficiency with which p-type WSe_2 can carry out reductive processes under illumination. Jakubowicz et al. observed significant improvements of the carrier-collection properties in p-WSe_2 samples that had been

dx.doi.org/10.1021/ja308581g | J. Am. Chem. Soc. 2013, 135, 223−231

subjected to a surface etching procedure.[19] Fan et al. used both p-WSe_2 and n-WSe_2 as dual light absorbers in a "rechargeable photoredox cell" energy-storage scheme that involved methyl viologen and polyiodide redox chemistry.[24] Cabrera and Abruña observed relatively high photovoltages, but low photocurrent densities, from polycrystalline p-WSe_2 in contact with outer-sphere, kinetically rapid, one-electron aqueous redox couples.[42] Figures 1−3 demonstrate that p-WSe_2 crystals synthesized in the presence of WO_2Cl_2 and Nb can effect efficient solar energy conversion in both fuel-forming and regenerative photoelectrochemical cells.

Without deposition of a hydrogen-evolution catalyst, the p-WSe_2 exhibited negligible photoelectrode energy-conversion efficiency for H_2 production. The related sulfide compounds, MoS_2 and WS_2, have recently been shown to exhibit significant electrocatalytic activities for hydrogen evolution.[15] However, the crystals used for the present study were selected to minimize the density of step edges, which are the active sites for hydrogen evolution in the related sulfide compounds. Thus, the relatively low electrocatalytic performance of these crystals toward hydrogen evolution does not preclude the possibility of obtaining reasonably efficient electrocatalysis from crystals that contain a high density of $MoSe_2$ or WSe_2 edge sites.

For the HER, Ru has a lower fundamental catalytic activity than Pt, which is consistent with the slower increase in cathodic current at $E < E_{oc}$ for p-WSe_2/Ru relative to p-WSe_2/Pt electrodes. However, Pt has a higher work function than Ru, resulting in less of an advantage from the "pinch-off" effect (i.e., preservation of a large effective barrier height) for a nanostructured catalyst film on the semiconductor surface.[43] Thus, the mixed Ru/Pt electrocatalyst system provided a balance of high catalytic activity and favorable interfacial energetics to markedly improve the solar energy-conversion efficiency.

In the best case, thermodynamically based photoelectrode energy-conversion efficiencies of >7% for hydrogen evolution under simulated 100 mW cm^{-2} of illumination were obtained using WSe_2 electrodes that had been coated with a mixed Ru/Pt electrocatalyst. These efficiencies are lower than those observed by Heller et al. for p-InP hydrogen-evolving photoelectrodes coupled to noble metal cocatalysts.[5,6,44] The difference can be ascribed to the lower photocurrent densities (relative to incoming light flux) and fill factors for the p-WSe_2 photoelectrodes described herein compared to the behavior of p-InP photocathodes. Optimization of crystal growth and catalyst deposition procedures will likely yield improved performance for p-WSe_2 photocathodes.

Reversible Photoelectrochemistry. The energy-conversion properties of p-WSe_2 in contact with the $Ru(NH_3)_6^{3+/2+}$ redox system indicate the extent to which the $J-E$ behavior exhibited by p-WSe_2 for the HER is limited by the crystalline semiconductor vs by the kinetics of the redox reaction. The $Ru(NH_3)_6^{3+/2+}$ redox couple is suitable for assessing the photoelectrode energy-conversion efficiency for p-WSe_2, owing to the relatively negative formal potential, stability under aqueous conditions, facile electron transfer kinetics, and high optical transparency of the redox system.

The illuminated $J-E$ response for the p-WSe_2/Ru-$(NH_3)_6^{3+/2+}$ contact contained essentially the same key features as those observed in the hydrogen-evolution experiments in 0.5 M H_2SO_4, exhibiting a well-defined open-circuit potential of >0.5 V relative to the Nernst potential of the solution, along with an increase of cathodic current density for $E < E_{oc}$. The photoelectrode energy-conversion efficiencies of p-WSe_2/Ru-$(NH_3)_6^{3+/2+}$ junctions, however, were somewhat lower than those for p-WSe_2−Ru/Pt/H_2O contacts in acidic media, due to lower fill factors in the former system (see Supporting Information). Similar V_{oc} values are to be expected, because the formal potential of the $Ru(NH_3)_6^{3+/2+}$ redox couple is close to E_{NHE}, which should result in very similar diode characteristics for both of these semiconductor-liquid interfaces. The lower fill factors for p-WSe_2 in contact with $Ru(NH_3)_6^{3+/2+}$ relative to the fill factors observed in contact with aqueous acid can be ascribed to concentration overpotentials that result from the low concentration of redox-active $Ru(NH_3)_6^{3+/2+}$ species in the solutions that were used for collection of the $J-E$ data.

Stability. Illuminated WSe_2 photoelectrodes have been shown to exhibit high stability under oxidative conditions in contact with aqueous polyhalide redox species.[21] Little information is available, however, regarding the stability of p-type WSe_2 under reducing conditions. The $MV^{2+/+}$ redox couple exhibits reasonable stability and facile kinetics over a large range of pH values, and thus provided a suitable system for assessment of the stability of WSe_2 under cathodic conditions at potentials close to, or negative of, RHE. The use of $MV^{2+/+}$ rather than the H^+/H_2 redox couple avoided complications that result from instability of the catalyst coating or from fouling of the catalyst due to the effects of impurities in the electrolyte solution.

The p-WSe_2 crystals were relatively robust in either acidic or alkaline media, exhibiting large photocurrents for several hours under reducing conditions in full, simulated sunlight. The photocurrent density produced by the p-WSe_2 electrode decayed slightly under both acidic and alkaline conditions. However, the methyl viologen radical cation species is somewhat unstable under these conditions, so the decay may be due to degradation of the semiconductor, or to increased light absorption by the solution as a result of the slow decomposition of the redox species. The optical micrographs of the crystal surface revealed the emergence of a few small lines or cracks in the crystal surface after the acid stability test, but essentially no further change was observable in the crystal surface after the stability tests in the alkaline environment. The observed cracks could be a result of photoetching, which would imply eventual complete degradation of the photoelectrode over long times.

Approximately 2.5 C (25 μmol electrons) of charge were passed through the WSe_2 crystal over the course of each stability experiment. Assuming a thickness of ∼50 μm (over twice the measured value from electron microscopy on another crystal from the same batch), the entire electrode contained ∼3 μmol of active material. Thus, a large change in the morphology of the sample would have been visible by optical microscopy if even a few percent of the total charge passed during the stability experiment went to corrosion of the crystal surface. Thus, we conclude that the WSe_2 crystal surface exhibits high stability under reducing conditions, similar to what has been observed previously for n-WSe_2 under oxidizing conditions.[21] These experiments do not, however, preclude the possibility of slow photoetching at step edges or defects in the crystal surface. Thus, further stability studies are warranted, using longer time periods to determine whether slow photoetching of the crystal surface occurs.

Mott−Schottky Analysis. The Mott−Schottky ($C_{diff}-E$) data exhibited a small amount of frequency dispersion, which resulted in a range of values for the slope of C^{-2}_{diff} vs E, but

dx.doi.org/10.1021/ja308581g | J. Am. Chem. Soc. 2013, 135, 223−231

produced a very narrow range of intercepts on the potential axis. The doping density values calculated from analysis of the C_{diff}–E data ranged from 5×10^{17} to 3×10^{18} cm^{-3} for the p-WSe_2 samples tested. The Mott–Schottky analysis also indicated that only some of the crystals exhibited variations in flat-band potential (E_{fb}) with pH. The surface step-edge density correlated with the pH dependence (Figures 6 and 7) with electrodes having the largest density of step edges also exhibiting the largest pH dependence of E_{fb}.

Pristine crystals of n-type WSe_2 have been reported to exhibit essentially no pH dependence of E_{fb}, whereas stepped surfaces exhibited a strong dependence of E_{fb} on pH for $1 < pH < 9$, which is the same trend as observed in the present study.[29] The average shift in E_{fb} from acidic to alkaline pH for stepped p-WSe_2 crystals was ~230 mV (see Supporting Information), which also agrees with the previous data for n-WSe_2.

Band-Edge Positions. The values of E_{fb} and of the doping densities obtained from the Mott–Schottky analysis allow construction of energy diagrams for p-WSe_2/H_2O junctions. Figure 10 presents such diagrams at different pH values, for the specific case of a pristine (low step-edge) surface.

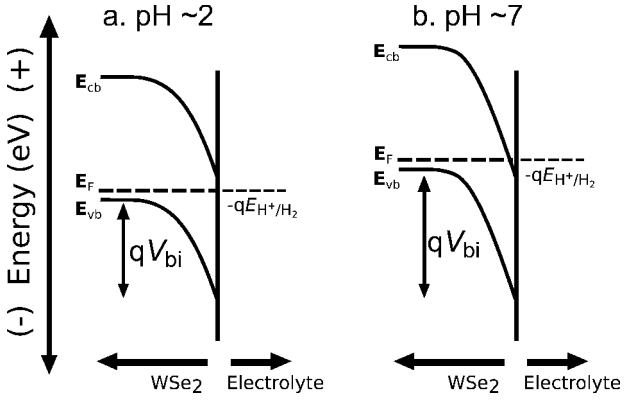

Figure 10. Idealized band diagram on an energy scale (e.g., energy vs vacuum) showing a pristine p-type WSe_2 electrode in equilibrium with the hydrogen-evolution potential in acidic (a) and neutral (b) aqueous electrolytes. The band-edge positions are insensitive to changes in pH over this range, whereas increases in the pH produced a negative shift in the hydrogen-evolution potential. As a result, when changing from pH 2 to pH 7, the built-in potential, V_{bi}, increased to the maximum allowed value, concomitant with the formation of a carrier inversion layer.

Under acidic conditions, the hydrogen-evolution potential is just positive of $\mathbf{E}_{cb}$ of WSe_2, (where the energy of the bottom of the conduction band, $\mathbf{E}_{cb}$, is related to the potential of the bottom of the conduction band, E_{cb} by $\mathbf{E}_{cb} = -qE_{cb}$) resulting in a large but not maximized built-in potential, V_{bi}. Upon increasing the pH to produce neutral conditions, the hydrogen-evolution potential shifts to more negative values, whereas the band edges of pristine WSe_2 samples do not shift. Hence, the hydrogen-evolution potential moves negatively with respect to E_{cb} (shown as a positive energy shift relative to $\mathbf{E}_{cb}$ in Figure 10), and thus, as a result of electrochemical equilibration, the semiconductor is driven into strong inversion.

Strong inversion is a desirable condition, as it maximizes the V_{bi} at the semiconductor–liquid interface. Additionally, strong inversion has been shown to decrease the impact of surface trap states,[45,46] which have been implicated as a major source of recombination in layered transition metal chalcogenides.[47] Thus, the presence of an inversion layer is consistent with the observed higher photocurrent densities and photopotentials for p-WSe_2 effecting the HER at pH = 4.2 as compared to in 0.5 M H_2SO_4 (Figure 2), or as compared to the reduction of $Ru(NH_3)_6^{3+}$ (Figure 3). Increasing the pH further, to alkaline conditions, will increase the thickness of the inversion layer on the WSe_2 near-surface, resulting in similarly favorable hydrogen-evolution behavior, provided that the crystal is sufficiently stable to provide robust electrochemical performance under such conditions.

For a moderately stepped WSe_2 crystal surface, the band edges remain fixed while the pH is varied from acidic to neutral conditions, resulting in a strong inversion layer at neutral pH. With continued increases in pH, the band edges will begin to shift in the negative direction, along with the RHE potential, but the strongly inverted surface layer remains. Stepped crystal surfaces, however, may exhibit other deleterious behaviors, such as spatially inhomogeneous barrier heights, which may result in poorer performance in spite of the favorable charge equilibration conditions. This conclusion is consistent with our results in that stepped surfaces consistently produced lower solar energy-conversion efficiencies than nonstepped surfaces, similar to the behavior reported previously for n-WSe_2.[47]

The pH dependence of the band edges in p-WSe_2 is significant, as it points toward ideal conditions for hydrogen evolution using this semiconductor. For strongly acidic solutions, the crystal is not in strong inversion and achievement of the highest possible V_{oc} would require use of a homojunction, heterojunction, or surface functionalization. However, under conditions ranging from mildly acidic to alkaline, the pristine crystal surface permits the formation of a strong inversion layer, allowing for the maximum photovoltage to be obtained even without surface functionalization or formation of a metallurgical junction. This large photovoltage is available even in the presence of a discontinuous catalyst layer on the surface, enabling efficient production of H_2 for $E >$ RHE. Indeed, the observed photovoltages of >0.6 V under mildly acidic conditions are comparable to those that have been observed for highly efficient n-WSe_2 electrodes in contact with polyiodide redox couples.[30,31]

Spectral Response. Spectral response data have been collected previously for n-type WSe_2 single crystals.[26] Our results generally match those of previous workers, indicating that the photocurrent yield is high for photon energies above the direct band gap of WSe_2. At energies near and below the direct band gap, however, the optical penetration depth increases into the bulk of the semiconductor and the quantum yield concomitantly decreases rapidly. This result implies that minority carriers generated in the bulk of the semiconductor cannot travel a sufficient distance to be collected at the solution interface and instead participate in recombination processes.

As shown in Figure 9, Gärtner-modeling of the spectral response of our p-WSe_2 samples indicated that the effective diffusion length for minority carriers (L_D) was ~1 μm. Similar analysis on n-type and p-type WSe_2, using both spectral response and electron-beam induced current (EBIC) measurements, has yielded values of L_D as high as 4 μm.[19]

A likely reason that the L_D values from our samples were somewhat lower than those observed previously is that significant care was not taken to ensure high purities for all of the starting materials. Additionally, the Mott–Schottky data indicate that these p-WSe_2 crystals were too heavily doped to produce optimum photoelectrochemical performance. The

dx.doi.org/10.1021/ja308581g | J. Am. Chem. Soc. 2013, 135, 223–231

doping densities that were calculated from the slopes of the Mott−Schottky data indicated nearly degenerate doping, based on a value of $\sim 10^{19}$ cm^{-3} for the effective density of states in the valence band of WSe_2.[48] The result is a very narrow space-charge region and a large concentration of impurity species that contribute to bulk recombination losses. Thus, decreasing the doping density (e.g., by decreasing the Nb loading in the growth ampule) and increasing the purity of the starting materials should increase the L_D, thereby enhancing the quantum yields at energies near the band gap of WSe_2 and providing still higher energy-conversion efficiencies than those reported herein.

The observed short-circuit cathodic photocurrent densities of p-WSe_2 electrodes for hydrogen evolution and for the reduction of $Ru(NH_3)_6^{3+}$ ranged from 15 to 25 mA cm^{-2}. These values are in accord with the photocurrent densities predicted from the spectral response data obtained for p-WSe_2-$MV^{2+/+}$ contacts. Assuming that the index of refraction of WSe_2 is $\sim$4.5,[40] reflection losses at the semiconductor/electrolyte interface could be as high as 30% for a perfectly smooth surface. Much of this reflection could be mitigated by judicious use of antireflective coatings and/or surface texturing. Additionally, effective L_D values as long as 4 μm have been observed in crystalline p-WSe_2, implying significantly lower bulk recombination losses than those in the crystals used in the present work.[19] Obtaining similar L_D values in p-WSe_2, through optimization of doping and minimization of impurities in the synthesis, should allow for collection of essentially all photons with energies above the direct band gap, and also should allow for collection of a larger proportion of photons with energies above the indirect gap of WSe_2. Photocurrent densities in excess of 30 mA cm^{-2} should therefore be possible for improved p-WSe_2 electrodes, resulting in solar energy-conversion efficiencies on the order of 10% or greater.

The most efficient hydrogen-evolving p-WSe_2 electrodes tested in the present work yielded V_{oc} values on the order of 630 mV. These values can be compared to what might be expected of photoelectrodes with improved quantum yields and carrier transport properties. The maximum V_{oc} values obtainable by p-WSe_2 electrodes can be estimated by the Shockley diode equation, assuming that bulk carrier recombination is the dominant limiting photovoltage process:[49]

$$V_{oc,max} \approx \frac{kT}{q} \ln\left[\frac{J_{ph} L_n N_A}{q D_n n_i^2}\right] \quad (2)$$

Equation 2 yields a $V_{oc,max}$ value of approximately 720 mV, where the terms and the associated values collected from either the present work or previous studies are as follows:[48] J_{ph} = 20 mA cm^{-2} is the light-limited photocurrent density; L_n = 1 μm is the minority-carrier diffusion length; $N_A = 10^{18}$ cm^{-3} is the dopant density; $q = 1.6 \times 10^{-19}$ C is the unsigned value of the elementary charge; D_n = 5 cm^2 s^{-1} is the minority-carrier diffusion coefficient; and $n_i = 1.5 \times 10^9$ cm^{-3} is the intrinsic carrier density of the semiconductor. Hence, the observed V_{oc} values are within 100 mV of the theoretical maximum value, assuming bulk carrier recombination is dominant. Nevertheless, the V_{oc} values can be improved toward the theoretical limit by increases in the material purity and quality, which would result in increases in J_{ph}, L_n, and thus V_{oc}.

CONCLUSIONS

Crystalline p-WSe_2 electrodes can reduce one-electron, outer-sphere redox couples stably for several hours under aqueous acidic or alkaline conditions. The band-edge alignment of p-WSe_2 with the hydrogen redox couple suggests that the maximum photovoltage available from this semiconductor can be achieved in solutions ranging from mildly acidic to strongly alkaline, owing to the pH-independence of the band-edge positions and the formation of a strong inversion layer. Open-circuit photovoltages of >600 mV, and overall thermodynamic photoelectrode solar energy-conversion efficiencies of >7%, have been achieved using noble metal composite catalysts on p-WSe_2 photocathodes. However, effective minority-carrier diffusion lengths of only $\sim$1 μm were observed, resulting in low quantum yields at photon energies below the direct band gap. Higher energy-conversion efficiencies should therefore be possible with better control of doping as well as with further increases in the crystal purity.

ASSOCIATED CONTENT

Supporting Information

Details and discussion of Mott−Schottky data analysis and diffusion length modeling. Current−voltage data, electron microscopy, and discussion of catalyst deposition. Comparison of ELH and AM1.5G light sources relative to spectral response results. Further discussion of hydrogen evolution energy-conversion efficiency calculations. Tabulated solar energy figures of merit for all redox couples. This material is available free of charge via the Internet at http://pubs.acs.org.

AUTHOR INFORMATION

Corresponding Author

*hbgray@caltech.edu; nslewis@caltech.edu

Notes

The authors declare no competing financial interest.

ACKNOWLEDGMENTS

This material is based upon work performed by the Joint Center for Artificial Photosynthesis, a DOE Energy Innovation Hub, supported through the Office of Science of the U.S. Department of Energy under Award Number DE-SC0004993. The contributions from JRM and HBG were supported by CCSER (the Gordon and Betty Moore Foundation). JRM is supported by a graduate research fellowship from the Office of Science of the U.S. Department of Energy.

REFERENCES

(1) Lewis, N. S.; Nocera, D. G. *Proc. Natl. Acad. Sci. U.S.A.* **2006**, *103*, 15729.
(2) Mallouk, T. E. *J. Phys. Chem. Lett.* **2010**, *1*, 2738.
(3) Whitesides, G. M.; Crabtree, G. W. *Science* **2007**, *315*, 796.
(4) Bard, A. J.; Whitesides, G. M.; Zare, R. N.; McLafferty, F. W. *Acc. Chem. Res.* **1995**, *28*, 91.
(5) Heller, A.; Vadimsky, R. G. *Phys. Rev. Lett.* **1981**, *46*, 1153.
(6) Aharon-Shalom, E.; Heller, A. *J. Electrochem. Soc.* **1982**, *129*, 2865.
(7) Boettcher, S. W.; Warren, E. L.; Putnam, M. C.; Santori, E. L.; Turner-Evans, D.; Kelzenberg, M. D.; Walter, M. G.; McKone, J. R.; Brunschwig, B. S.; Atwater, H. A.; Lewis, N. S. *J. Am. Chem. Soc.* **2010**, *133*, 1216.
(8) Walter, M.; Warren, E.; McKone, J.; Boettcher, S.; Qixi, M.; Santori, L.; Lewis, N. *Chem. Rev.* **2010**, *110*, 6446.

(9) Hernández-Pagán, E. a.; Vargas-Barbosa, N. M.; Wang, T.; Zhao, Y.; Smotkin, E. S.; Mallouk, T. E. *Energy Environ. Sci.* **2012**, *5*, 7582.
(10) Baglio, J. A.; Calabrese, G. S.; Harrison, D. J.; Kamieniecki, E.; Ricco, A. J.; Wrighton, M. S.; Zoski, G. D. *J. Am. Chem. Soc.* **1983**, *105*, 2246.
(11) Douay, V.; Gorochov, O. *J. Chem. Phys.* **1986**, *83*, 247.
(12) Sobczynski, A.; Yildiz, A.; Bard, A. J.; Campion, A.; Fox, M. A.; Mallouk, T.; Webber, S. E.; White, J. M. *J. Phys. Chem.* **1988**, *92*, 2311.
(13) Bonde, J.; Moses, P. G.; Jaramillo, T. F.; Norskov, J. K.; Chorkendorff, I. *Faraday Discuss.* **2008**, *140*, 219.
(14) Chen, Z.; Cummins, D.; Reinecke, B.; Clark, E. L.; Mahendra, S.; Jaramillo, T. F. *Nano Lett.* **2011**, *11*, 4168.
(15) Jaramillo, T. F.; Jørgensen, K. P.; Bonde, J.; Nielsen, J. H.; Horch, S.; Chorkendorff, I. *Science* **2007**, *317*, 100.
(16) Merki, D.; Fierro, S.; Vrubel, H.; Hu, X. *Chem. Sci.* **2011**, *2*, 1262.
(17) Szklarczyk, M.; Bockris, J. O. *Int. J. Hydrogen Energy* **1984**, *9*, 831.
(18) Vrubel, H.; Merki, D.; Hu, X. *Energy Environ. Sci.* **2012**, *5*, 6136.
(19) Jakubowicz, A.; Mahalu, D.; Wolf, M.; Wold, A.; Tenne, R. *Phys. Rev. B* **1989**, *40*, 2992.
(20) Sourisseau, C.; Cruege, F.; Gorochov, O. *J. Electroanal. Chem.* **1991**, *308*, 239.
(21) Kline, G.; Kam, K.; Canfield, D.; Parkinson, B. A. *Sol. Energy Mater.* **1981**, *4*, 301.
(22) Aruchamy, A. *Photoelectrochemistry and Photovoltaics of Layered Semiconductors*; Springer, 1992.
(23) Srivastava, S. K.; Avasthi, B. N. *J. Mater. Sci.* **1985**, *20*, 3801.
(24) Fan, F.-R. F.; White, H. S.; Wheeler, B. L.; Bard, A. J. *J. Am. Chem. Soc.* **1980**, *102*, 5142.
(25) Kautek, W.; Gerischer, H.; Tributsch, H. *J. Electrochem. Soc.* **1980**, *127*, 2471.
(26) Kam, K. K.; Parkinson, B. A. *J. Phys. Chem.* **1982**, *86*, 463.
(27) Kline, G.; Kam, K. K.; Ziegler, R.; Parkinson, B. A. *Sol. Energy Mater.* **1982**, *6*, 337.
(28) Levy-Clement, C.; Heller, A.; Bonner, W. A.; Parkinson, B. A. *J. Electrochem. Soc.* **1982**, *129*, 1701.
(29) Lewerenz, H. J.; Gerischer, H.; Lubke, M. *J. Electrochem. Soc.* **1984**, 100.
(30) Tenne, R.; Wold, A. *Appl. Phys. Lett.* **1985**, *47*, 707.
(31) Prasad, G.; Srivastava, O. N. *J. Phys. D: Appl. Phys.* **1988**, *21*, 1028.
(32) Mahalu, D.; Jakubowicz, A.; Wold, A.; Tenne, R. *Phys. Rev. B* **1988**, *38*, 1533.
(33) Mahalu, D.; Margulis, L.; Wold, A.; Tenne, R. *Phys. Rev. B* **1992**, *45*, 1943.
(34) Baglio, J.; Kamieniecki, E.; Decola, N.; Struck, C.; Marzik, J.; Dwight, K.; Wold, A. *J. Solid State Chem.* **1983**, *49*, 166.
(35) Kershaw, R.; Vlasse, M.; Wold, A. *Inorg. Chem.* **1967**, *6*, 1599.
(36) Koval, C. A.; Olson, J. B. *J. Electroanal. Chem.* **1987**, *234*, 133.
(37) Klein, A.; Dolatzoglou, P.; LuxSteiner, M.; Bucher, E. *Sol. Energy Mater. Sol. Cells* **1997**, *46*, 175.
(38) Legma, J. B.; Vacquier, G.; Casalot, A. *J. Cryst. Growth* **1993**, *130*, 253.
(39) Casagrande, L. G.; Tufts, B. J.; Lewis, N. S. *J. Phys. Chem.* **1991**, *95*, 1373.
(40) Antoci, S.; Camagni, P.; Manara, A.; Stella, A. *J. Phys. Chem. Solids* **1972**, *33*, 1177.
(41) Deshpande, M. P.; Solanki, G. K.; Agarwal, M. K. *Mater. Lett.* **2000**, *43*, 66.
(42) Cabrera, C. R.; Abruna, H. D. *J. Electrochem. Soc.* **1988**, *135*, 1436.
(43) Rossi, R. C.; Lewis, N. S. *J. Phys. Chem. B* **2001**, *105*, 12303.
(44) Heller, A.; Aharon-Shalom, E.; Bonner, W. A.; Miller, B. *J. Am. Chem. Soc.* **1982**, *104*, 6942.
(45) Royea, W. J.; Michalak, D. J.; Lewis, N. S. *Appl. Phys. Lett.* **2000**, *77*, 2566.
(46) Michalak, D. J.; Lewis, N. S. *Appl. Phys. Lett.* **2002**, *80*, 4458.
(47) Lewerenz, H. J.; Heller, A.; Disalvo, F. J. *J. Am. Chem. Soc.* **1980**, *102*, 1877.
(48) Solanki, G. K.; Gujarathi, D. N.; Deshpande, M. P.; Lakshminarayana, D.; Agarwal, M. K. *Cryst. Res. Technol.* **2008**, *43*, 179.
(49) Lewis, N. S. *J. Electrochem. Soc.* **1984**, *131*, 2496.